Molecular Therapy
Nucleic Acids
Original Article

Icariin attenuates endothelial-mesenchymal transition via H19/miR-148b-3p/ELF5 in ox-LDL-stimulated HUVECs

Shan Liu,[1] Dong-sheng Xu,[2] Min Li,[1] Yang Zhang,[1] Qi Li,[1,3] Teng-teng Li,[1] and Li-qun Ren[1]

[1]Department of Experimental Pharmacology and Toxicology, School of Pharmacy, Jilin University, Changchun 130021, Jilin Province, China; [2]Cancer Center, The First Hospital of Jilin University, Changchun 130021, Jilin Province, China; [3]The Third Hospital Affiliated of Jinzhou Medical University, Jinzhou 121000, Liaoning, China

Atherosclerosis is the main cause of cardio-cerebrovascular diseases. Endothelial-mesenchymal transition plays an important role in atherosclerosis. Icariin has a protective effect on atherosclerosis; however, the underlying mechanism remains unclear. In this study, we explored the molecular mechanism underlying the protective function of icariin in oxidized low-density lipoprotein-stimulated human umbilical vein endothelial cells. H19, a long non-coding RNA, was identified to be downregulated in the background of the oxidized low-density lipoprotein-induced endothelial-mesenchymal transition in human umbilical vein endothelial cells. Icariin upregulated H19 expression and inhibited the transformation of endothelial cells into interstitial cells. Overexpression of H19 affected endothelial-mesenchymal transition in oxidized low-density lipoprotein-stimulated human umbilical vein endothelial cells, whereas H19 knockdown reversed endothelial protective effects of icariin and reduced human umbilical vein endothelial cell migration. Knockdown of H19 significantly downregulated oxidized low-density lipoprotein-induced E74-like factor 5 and upregulated miR-148b-3p, which was reversed by icariin. Thus, icariin may play a protective role in atherosclerosis, and H19 may be a potential therapeutic target.

INTRODUCTION

In recent years, with changes in lifestyle and dietary habits, the incidence and mortality rates of cardiovascular and cerebrovascular diseases caused by atherosclerosis (AS) have increased annually, becoming the main cause of death.[1] AS is a complicated chronic disease characterized by lipid deposition in the blood vessel wall, involving an inflammatory and proliferative cascade of functional cells, including smooth muscle, endothelial, and immune cells.[2] The formation of AS plaque is not only related to lipid deposition in the blood vessel walls but also closely related to the accumulation of arterial intima mesenchymal cells. The origin of new endometrial mesenchymal cells in plaques has received widespread attention.[3–5] Studies have shown that these new mesenchymal cells originate from endothelial cells in large numbers.[6] AS can easily damage the vascular endothelium, and this damage changes the endothelial cell phenotype such that it acquires interstitial properties. During this process, endothelial cells gradually lose their morphology and function and acquire the phenotype and characteristics of mesenchymal cells with respect to proliferation, migration, and collagen synthesis, a process referred to as endothelial-mesenchymal transition (EndMT).[4] Recently, an increasing number of studies have shown that EndMT plays an important role in AS.

Icariin (ICA) is one of the active ingredients of *Epimedium*. There is extensive research on its pharmacological activities, including anti-inflammatory, anti-osteoporotic, and immune regulatory effects.[7,8] In recent years, researchers have conducted several studies on the anti-AS effect of ICA, confirming the protective effect of ICA on the cardiovascular system, but its specific targets, related biological processes, and signal transduction pathways need further exploration.

Long non-coding RNAs (lncRNAs) exist in the nucleus or cytoplasm without a full open reading frame (ORF). Studies have shown that most lncRNAs contain conserved regions, which affect gene expression via genomic imprinting, chromatin compensation, X chromosome inactivation, and epigenetic modification.[9,10] lncRNAs play an important role in various diseases. lncRNA H19 is paternally imprinted but maternally expressed. Brannan et al.[11] revealed that the three ORFs of H19 contain many translational termination signals but no clear protein-coding sections. Thus, it was proposed that H19 mRNA only encodes RNA and not protein. lncRNA H19 is widely expressed in various tissues and cells and exerts its effects via various regulatory modes.[12] We previously showed upregulated lncRNA H19 expression upon ICA intervention in mice. The mechanism underlying H19 involvement in AS remains unclear. Zhu et al.[13] identified a miR-148b-3p-binding site in H19 and found that the binding leads to decreased H19 expression in human hepatic sinusoidal endothelial cells. Zhang et al.[14] demonstrated that miR-148b-3p inhibits the pro-angiogenic phenotype of endothelial cells. Hence, we hypothesized that miR-148b-3p contributes to the effect

Received 18 September 2020; accepted 27 November 2020;
https://doi.org/10.1016/j.omtn.2020.11.021.

Correspondence: Li-qun Ren, Department of Experimental Pharmacology and Toxicology, School of Pharmacy, Jilin University, 1266 Fujin Road, Changchun 130021, Jilin Province, China.
E-mail: renliqun406@hotmail.com

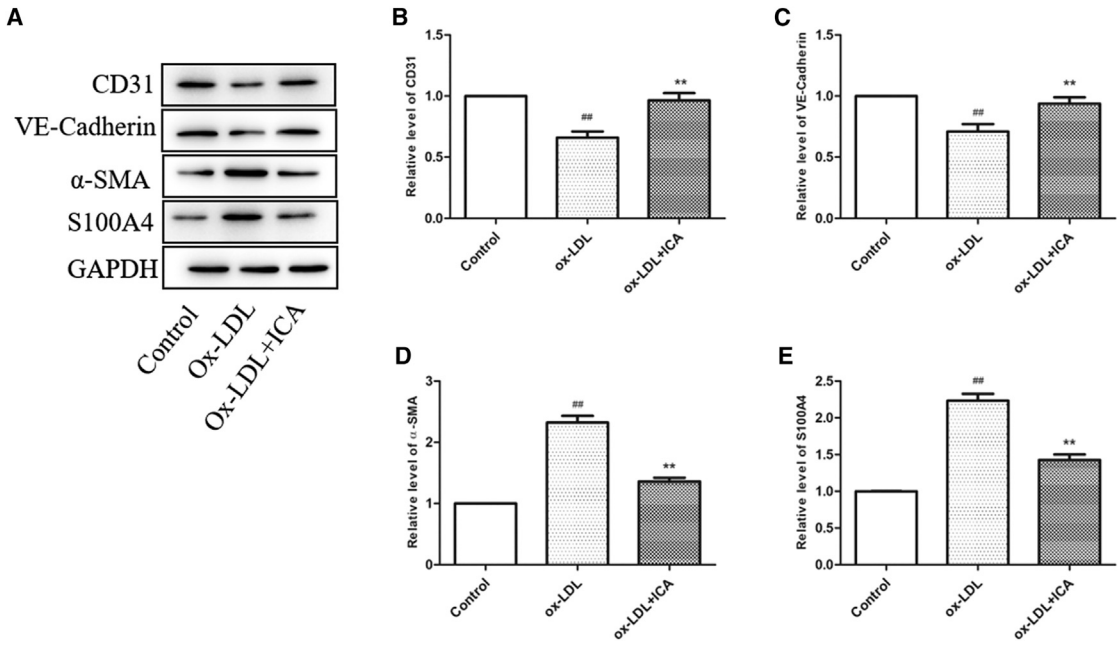

Figure 1. ICA suppressed ox-LDL-induced EndMT in HUVECs

(A–E) Expression levels of CD31, VE-cadherin, α-SMA, and S100A4 in HUVECs exposed to 200 μM ox-LDL or ox-LDL+10 μM ICA, determined using western blotting. $^{\#\#}p < 0.01$ versus control group; $^{**}p < 0.01$ versus ox-LDL group; n = 3. Measurement data are expressed as mean ± SD. ICA, icariin; ox-LDL, oxidized low-density lipoprotein; EndMT, endothelial-mesenchymal transition; HUVEC, human umbilical vein endothelial cell.

of H19 in AS. E74-like factor 5 (ELF5) plays a vital role in cell differentiation and tissue formation.[15,16] Moreover, ELF5 inhibits EndMT, and miR-148b-3p was predicted to bind to the ELF5 3′ UTR. In the present study, we investigated the role of H19, miR-148b-3p, and ELF5 in oxidized low-density lipoprotein (ox-LDL)-induced AS in human umbilical vein endothelial cells (HUVECs).

RESULTS

ICA suppressed ox-LDL-induced EndMT in HUVECs

To verify the effects of ICA on ox-LDL-induced EndMT in HUVECs, we treated HUVECs with ox-LDL or ox-LDL+ICA. Specific proteins of endothelial cells (such as vascular endothelial cadherin [VE-cadherin] and CD31) and specific proteins of mesenchymal cells (such as α-smooth muscle actin [α-SMA] and S100A4) were detected using western blot analysis. As shown in Figure 1, ICA inhibited the expression of specific proteins in mesenchymal cells (α-SMA and S100A4) and upregulated the expression of specific proteins in endothelial cells (VE-cadherin and CD31).

ICA promoted ox-LDL-induced H19 expression in HUVECs

Our previous research has confirmed that ICA increases the expression of H19 in ApoE$^{-/-}$ mouse arteries. In order to explore the mechanism of ICA-induced inhibition of EndMT further, we studied the effects of ICA on EndMT-related molecules. The data showed that H19 expression was markedly decreased in HUVECs stimulated using ox-LDL. However, ICA increased the expression of H19 in HUVECs exposed to ox-LDL (Figure 2A). To further examine the role of H19 in EndMT, we modified H19 expression using pLVX-H19 and short hairpin RNA (shRNA) against H19 sh-H19 (Figure 2B). Our data indicated that H19 overexpression inhibited EndMT, as evidenced by enhanced VE-cadherin and CD31 expression and downregulated the expression of α-SMA and S100A4. In contrast, sh-H19 promoted EndMT, as evidenced by enhanced α-SMA and S100A4 expression and downregulated expression of VE-cadherin and CD31 (Figures 2C–2G). In the meantime, wound-healing (Figure 2H) and transwell assays (Figure 2I) proved that H19 overexpression reduced the migration of HUVECs and that sh-H19 reversed this effect. These results suggested that the aberrant expression of H19 was involved in ox-LDL-induced EndMT of HUVECs.

H19 knockdown attenuated EndMT inhibition by ICA

We further explored whether H19 is involved in EndMT inhibition by ICA. The results showed that ICA inhibited EndMT, as evidenced by enhanced VE-cadherin and CD31 expression, and downregulated the expression of α-SMA and S100A4 (Figures 3A–3E), as well as reduced the migration ability of HUVECs (Figures 3F and 3G), while H19 knockdown reversed the inhibitory effect of ICA on EndMT. These findings revealed that H19 played a crucial role in the inhibition of EndMT by ICA.

ICA regulated miR-148b-3p and ELF5 expression in HUVECs by upregulating H19

We also demonstrated that the upregulation of miR-148b-3p expression (Figure 4A) and reduction of ELF5 expression at the mRNA and

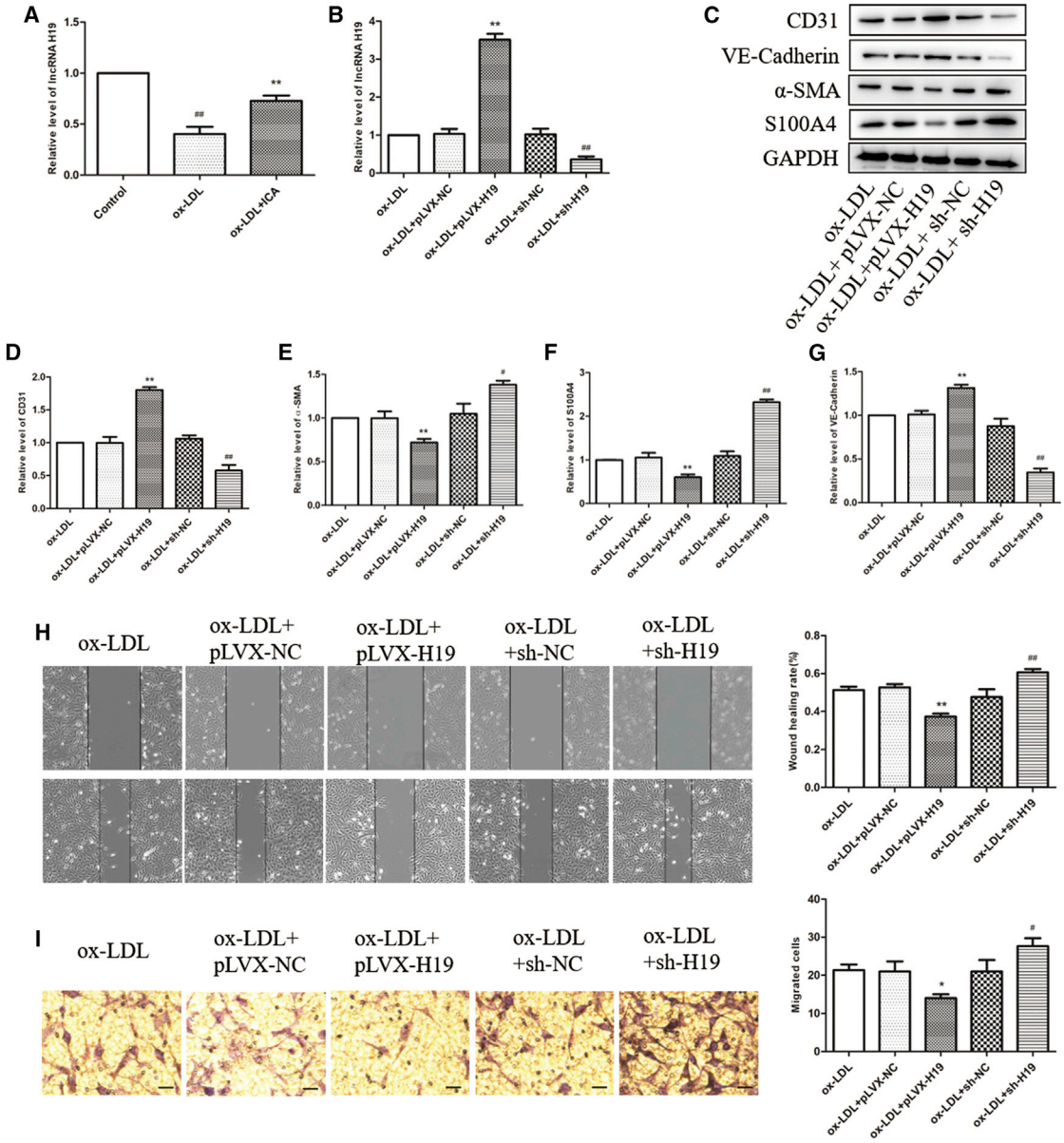

Figure 2. ICA promoted ox-LDL-induced H19 expression, and H19 affected EndMT in HUVECs

(A) The expression of H19 in HUVECs in control, ox-LDL, or ox-LDL+ICA groups was detected using quantitative real-time PCR. (B) Following transfection with recombinant H19 plasmids or sh-H19, the expression of H19 was detected using quantitative real-time PCR. (C–G) The expression of CD31, VE-cadherin, α-SMA, and S100A4 in ox-LDL-treated HUVECs was determined using western blot analysis. (H) Transwell assays were used to assess the migration capacity of HUVECs incubated for 24 h. (I) HUVECs were incubated for 24 h and subjected to a wound-healing assay to assess cell migration. Images were acquired at 0 and 24 h. *$p < 0.05$, **$p < 0.01$ versus pLVX-negative control (NC) group; $^{\#}p < 0.05$, $^{\#\#}p < 0.01$ versus sh-NC group; n = 3. Measurement data are expressed as mean ± SD. Scale bars, 100 μm.

protein levels (Figures 4B and 4C) in HUVECs treated with ox-LDL were reversed by ICA. Hence, we next aimed to estimate whether H19 regulates the expression of miR-148b-3p and ELF5. The results demonstrated that low expression of H19 caused a significant increase in miR-148b-3p expression (Figures 4D and 4E) and resulted in ELF5 downregulation (Figures 4F and 4G), while ICA led to a contrary effect.

H19 positively regulated the expression of ELF5 by regulating miR-148b-3p transcription

Bioinformatic analyses predicted that H19 and miR-148b-3p targeted each other, but the role of miR-148b-3p in AS was not confirmed. More importantly, bioinformatics-based prediction showed that miR-148b-3p could bind to ELF5 (a key transcription factor in EndMT), a member of the E26 transformation-specific (ETS)

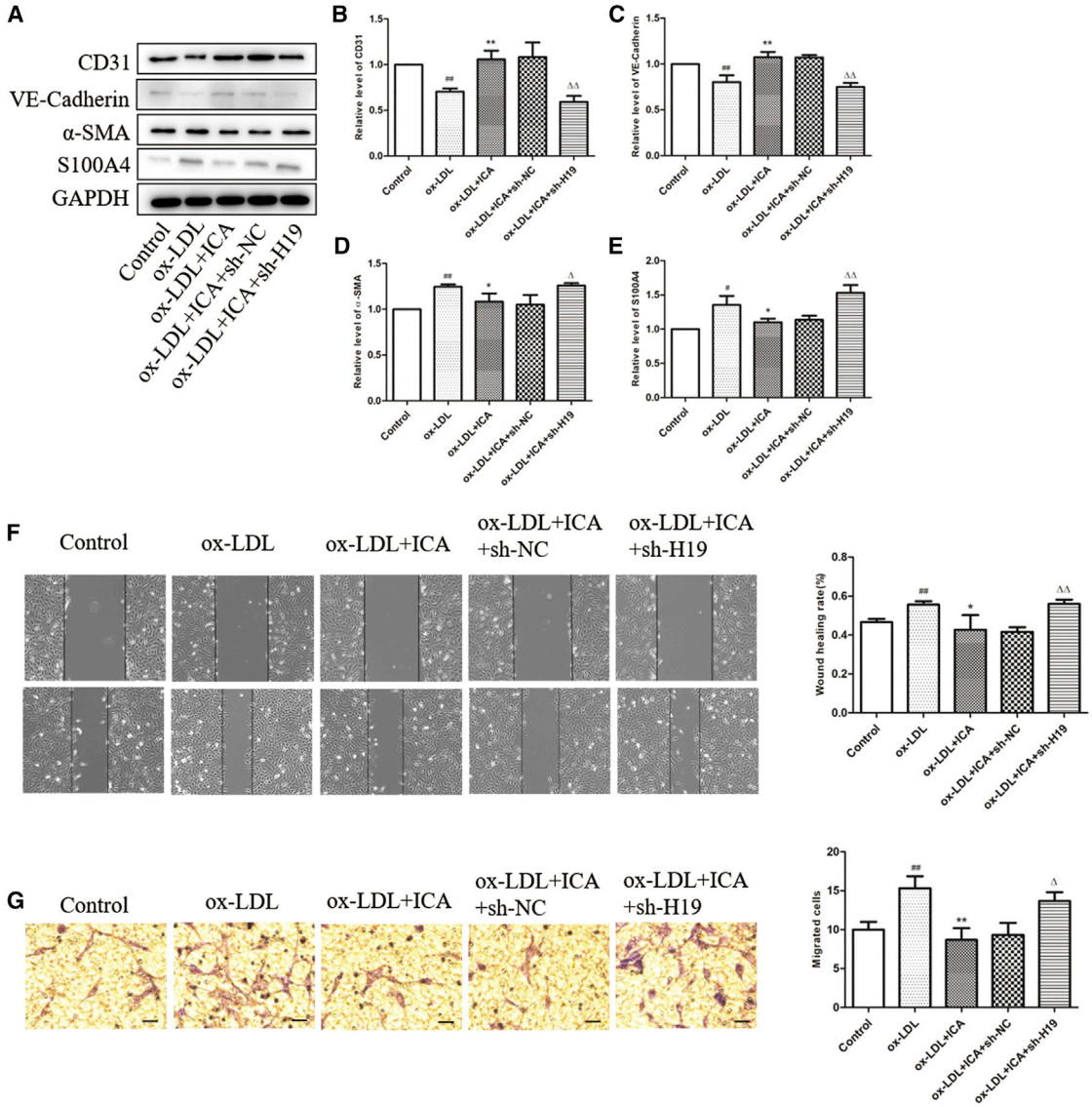

Figure 3. H19 knockdown attenuated the inhibitory effect of ICA on EndMT

(A–E) Western blot analysis was performed to detect the expression of CD31, VE-cadherin, α-SMA, and S100A4 in HUVECs. (F and G) Transwell (F) and wound-healing assays (G) were used to assess cell migration in HUVECs treated with ox-LDL with or without ICA for 24 h. $^{\#}p < 0.05$, $^{\#\#}p < 0.01$ versus control group; $^{*}p < 0.05$, $^{**}p < 0.01$ versus ox-LDL group; $^{\Delta}p < 0.05$, $^{\Delta\Delta}p < 0.01$ versus ox-LDL+ICA+sh-NC group; n = 3. Measurement data are expressed as mean ± SD. Scale bars, 100 μm.

transcription factor family with epithelial specificity, and the deletion of ELF5 might lead to EndMT. Thus, it was hypothesized that H19, miR-148b-3p, and ELF5 might form an axis that modulates EndMT in AS. We performed dual-luciferase reporter assays and found that the miR-148b-3p mimic significantly reduced H19- and ELF5 3′ UTR-dependent luciferase activity but did not influence the luciferase activity of the mutant reporter (Figures 5A and 5B). Notably, H19 overexpression decreased the expression of miR-148b-3p (Figure 5C) and upregulated ELF5 mRNA (Figure 5D) and protein expression (Figure 5E) while inhibiting H19-upregulated miR-148b-3p and H19-downregulated ELF5 expression, indicating that H19 regulated the transcription of miR-148b-3p to positively modulate ELF5 expression level in HUVECs. However, abnormal expression of miR-148b-3p inhibited H19-induced depletion of miR-148b-3p (Figure 5F) and ELF5 upregulation (Figures 5G and 5H). These data revealed that H19 could function as an endogenous miR-148b-3p sponge that regulated ELF5 expression.

ICA repressed EndMT by regulating the H19/miR-148b-3p/ELF5 axis

We then verified whether the inhibitory effect of ICA on EndMT was achieved through the H19/miR-148b-3p/ELF5 axis. We investigated

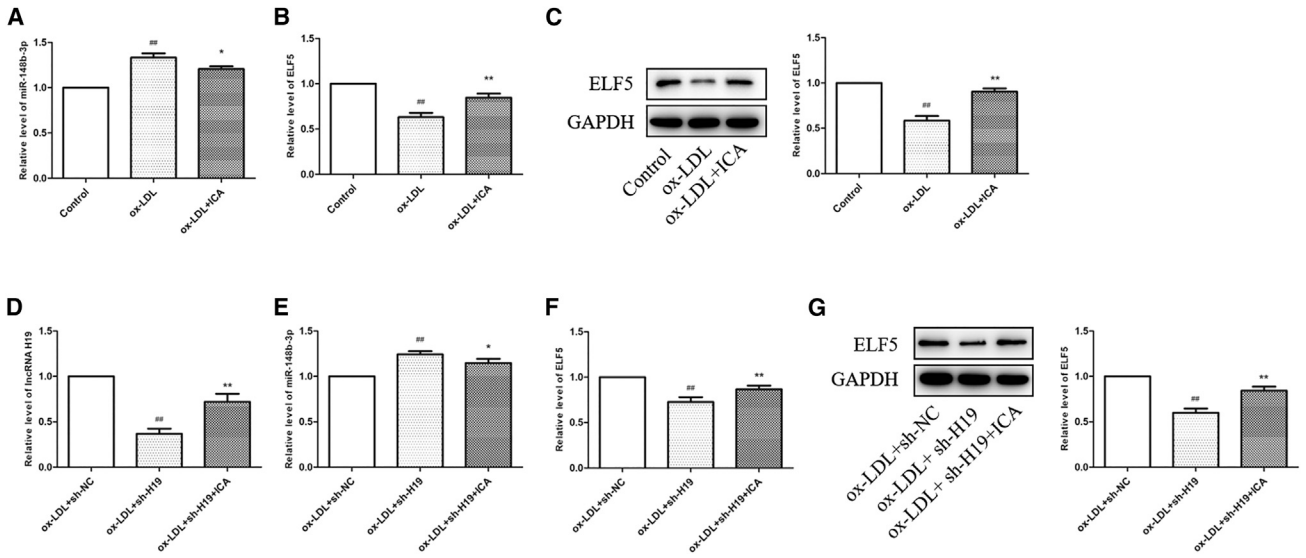

Figure 4. ICA regulated ox-LDL-mediated miR-148b-3p and ELF5 expression in HUVECs by upregulating H19

(A–C) miR-148b-3p (A) as well as ELF5 mRNA (B) and protein (C) expression levels in HUVECs in control and ox-LDL (with or without ICA) groups. $^{\#}p < 0.05$, $^{\#\#}p < 0.01$ versus control group; $^{*}p < 0.05$, $^{**}p < 0.01$ versus ox-LDL group; n = 3. (D–G) H19 (D), miR-148b-3p (E), and ELF5 mRNA (F) and protein (G) expression levels in HUVECs transfected with vector (sh-NC) and sh-H19, together with ICA treatment. $^{\#\#}p < 0.01$ versus sh-NC group; $^{*}p < 0.05$, $^{**}p < 0.01$ versus sh-H19 group; n = 3. Measurement data are expressed as mean ± SD.

the mechanism by which miR-148b-3p regulated EndMT development. As presented in Figures 6A–6G, H19 upregulation inhibited EndMT, as evidenced by elevated VE-cadherin and CD31 expression and downregulated expression of α-SMA and S100A4, and reduced the migration ability of HUVECs, while the miR-148b-3p mimic restored the related protein expression and migration of HUVECs. Finally, we investigated the role of ELF5 in EndMT. As shown in Figures 7A–7J, ELF5 knockdown partly reversed the inhibitory effect of H19 on EndMT. These results showed that H19 negatively regulated miR-148b-3p expression to inhibit EndMT of HUVECs by upregulating ELF5.

ICA inhibited the activation of TGF-β by regulating H19 expression to suppress EndMT

Transforming growth factor-β (TGF-β) plays a key role in EndMT and is mainly involved in regulating cell proliferation and differentiation. In our present study, we explored whether ICA affects the expression of TGF-β via the H19 axis to inhibit EndMT. The results showed that ICA inhibited TGF-β expression, which was increased by ox-LDL, while H19 knockdown restored TGF-β expression (Figure 8A). To further clarify the role of TGF-β in EndMT, we added galunisertib (TGF-β receptor inhibitor) to the cells, and our data showed that galunisertib significantly inhibited the expression of TGF-β and reversed the promoting effect of sh-H19 on EndMT, as evidenced by the upregulated expression of VE-cadherin and CD31 and downregulated expression of α-SMA and S100A4 (Figures 8B–8G).

DISCUSSION

Cardiovascular disease is a major threat to human health with high morbidity and mortality worldwide, and AS is an important pathological process leading to coronary atherosclerotic heart disease. Therefore, research aimed at regulating the progression of AS is of great significance for preventing and treating cardiovascular disease. Recent studies have found that EndMT plays a key role in regulating endothelial function and the development and structural remodeling of the myocardium, blood vessels, and valves, suggesting that it has important research significance in the field of cardiovascular diseases.

EndMT is a biological process in which endothelial cells are stimulated by external factors to change their characteristics and gain a mesenchymal cell or myofibroblast phenotype and express mesenchymal cell proteins.[17–19] EndMT can lead to plaque calcification, fibrous cap thinning, and increased plaque instability.[20] Researchers have always thought that the cells in the plaque are composed of macrophages, smooth muscle cells, and foam cells, which are formed after these cells engulf lipids. Recent studies have observed endothelial cells that undergo EndMT in the plaque.[4,21] This transition may be because the endothelial cells that undergo EndMT exhibit the migration properties of mesenchymal cells. Therefore, these cells pass through the arterial intima and enter the AS plaque and cooperate with other cells to promote plaque formation in the diseased part of AS. Unstable plaque may pose a serious threat to the patient's life. If a plaque is unstable, it will rupture, form a thrombus, and block arteries, causing myocardial infarction and unstable angina pectoris. Therefore, controlling plaque stability is an important way to prevent adverse cardiovascular events. Through the detection of different types of plaque fiber cap thickness and the number of endothelial cells that underwent EndMT in the plaque, Evrard et al.[3] found that the existence of the two was negatively correlated; that is, the higher the number

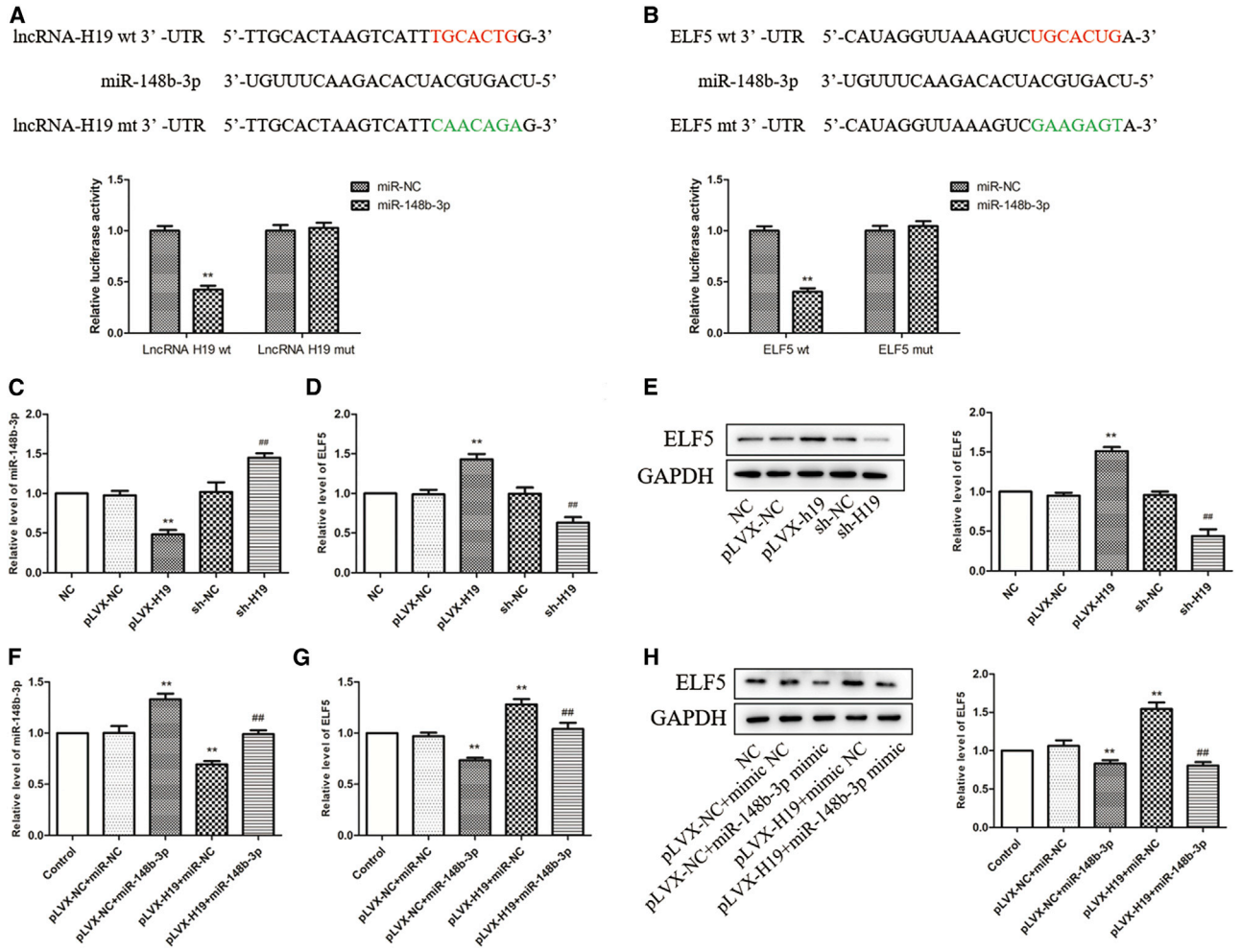

Figure 5. H19 positively regulated the ELF5 expression by sponging miR-148b-3p

(A and B) The relative luciferase activity in 293T cells co-transfected with miR-148b-3p mimic, NC, and wild-type mimics, or mutant (Mut) vector plasmids of H19 (A) or the ELF5 3′ UTR (B). **p < 0.01 versus miR-NC group; n = 3. (C–E) miR-148b-3p (C) as well as ELF5 mRNA (D) and protein (E) expression levels in HUVECs transfected with pLVX-H19, sh-H19, or their NCs. **p < 0.01 versus pLVX-NC group; ##p < 0.01 versus sh-NC group; n = 3. (F–H) miR-148b-3p (F) as well as ELF5 mRNA (G) and protein (H) expression levels in HUVECs co-transfected with vector or H19 and NC mimic or miR-148b-3p mimic. **p < 0.01 versus pLVX-NC+miR-NC group; ##p < 0.01 versus pLVX-H19+miR-NC group; n = 3. Measurement data are expressed as mean ± SD.

of EndMT endothelial cells in the plaque, the worse the stability. EndMT may be a key link in the prevention and treatment of AS. Cheng et al.[22] found that knocking out *wnt7* could promote AS calcification and that this effect is related to the upregulation of EndMT in human aortic endothelial cells. Hyperlipidemia is a key factor in the formation of AS, and studies have shown that ox-LDL promotes EndMT of human aortic endothelial cells and damages endothelial cell function.[23]

As one of the main active compounds of *Epimedium*, ICA reportedly demonstrates an anti-AS effect. ICA delays the progression of AS by inhibiting biological processes, such as oxidative damage, immune response, and chemotaxis.[24–28] Wang and Huang[29] found that ICA reduces oxidative stress damage in endothelial cells. Xiao-Hong et al.[30] confirmed that ICA reduces the level of reactive oxygen species and delays endothelial cell senescence induced by homocysteine. To date, few studies have examined the underlying role of ICA in AS. Our current study showed that ICA could inhibit ox-LDL-induced EndMT, thereby supporting the hypothesis that ICA exerts an endothelial protective effect *in vitro*.

lncRNAs play an important role in regulating endothelial cells, macrophages, vascular smooth muscle cells, vascular inflammation, and lipid metabolism. In recent years, studies have provided strong evidence that non-coding RNAs play vital roles in the occurrence and development of AS.[10] H19 was the first lncRNA to be discovered. *H19* is an imprinted gene with paternal imprinting characteristics that can selectively express maternal alleles. Studies have shown

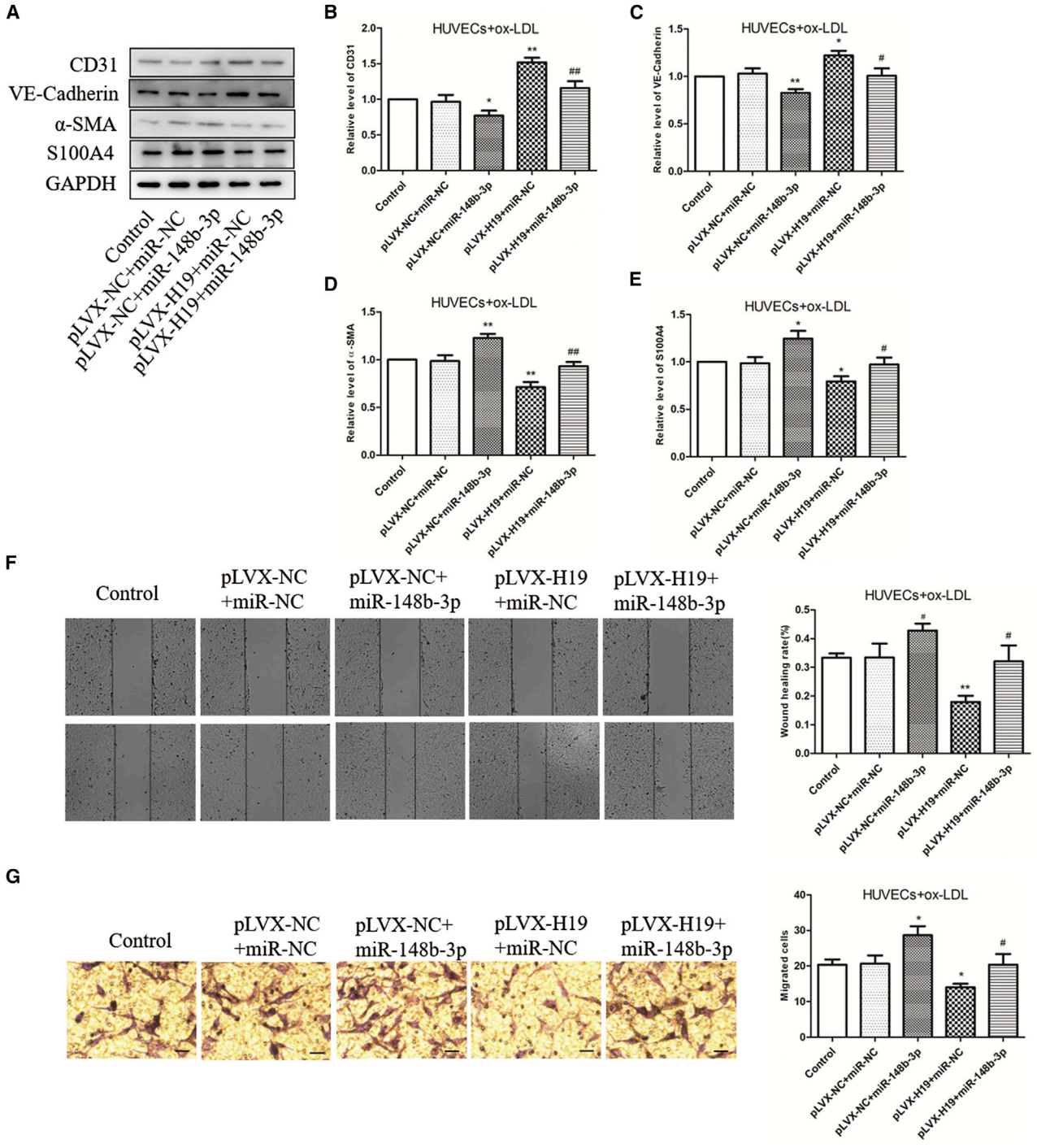

Figure 6. miR-148b-3p overexpression reversed H19-mitigated EndMT in ox-LDL-treated HUVECs

Cells were transfected with H19 plasmids or miR-148b-3p mimic and exposed to ox-LDL. (A–E) After that, the expression levels of CD31, VE-cadherin, α-SMA, and S100A4 in HUVECs were determined using western blot analysis. (F and G) Cell migration capacity was measured using wound-healing (F) and transwell assays (G). *$p < 0.05$, **$p < 0.01$ versus pLVX-NC+miR-NC group; $^{\#}p < 0.05$, $^{\#\#}p < 0.01$ versus pLVX-H19+miR-NC group; n = 3. Measurement data are expressed as mean ± SD. Scale bars, 100 μm.

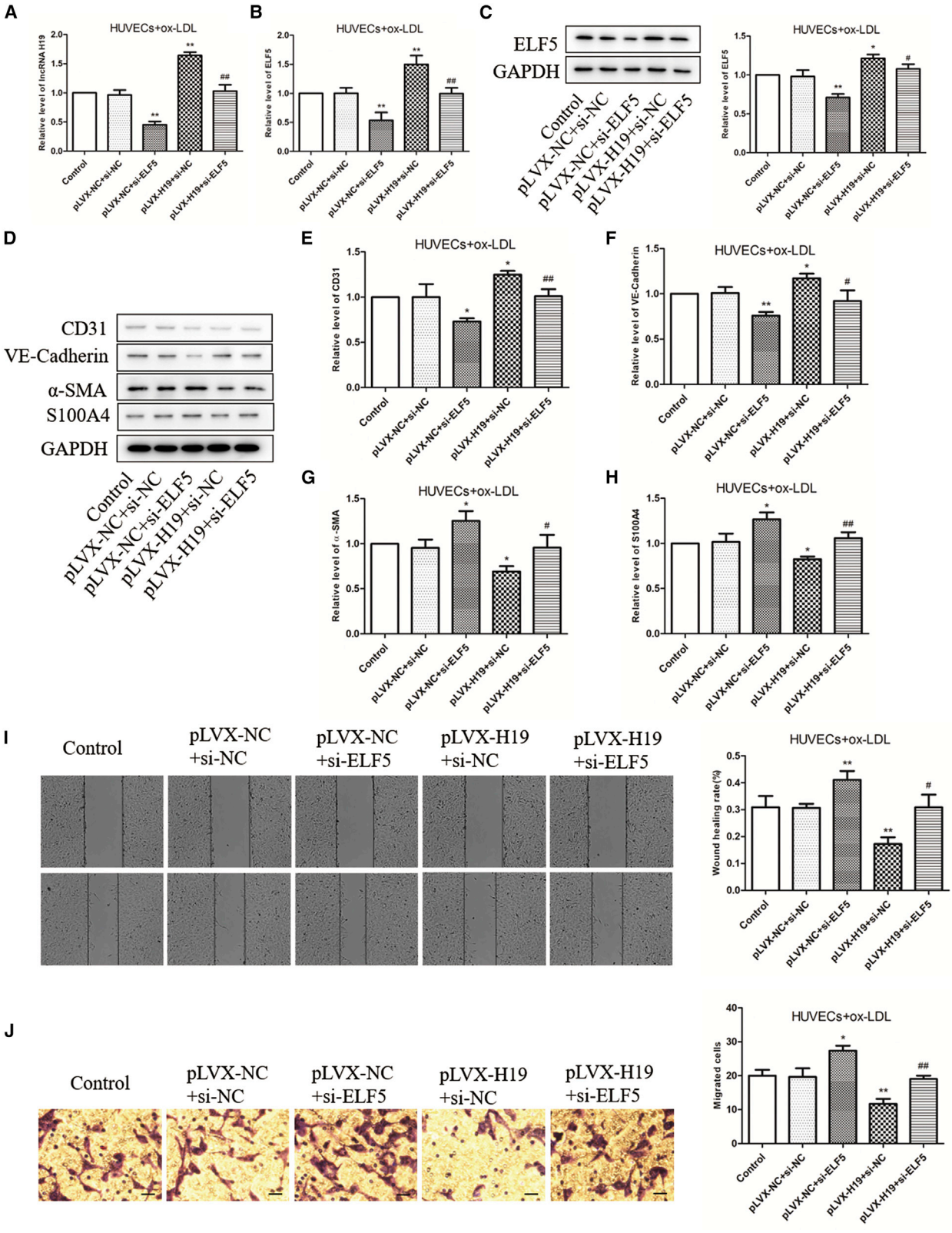

(legend on next page)

that H19 is highly expressed in various tumors and is closely related to tumor metastasis and prognosis.[31,32] However, H19 has different effects on different diseases, and the mechanism is also different. It is regulated by multiple factors. Conigliaro et al.[33] found that H19 could be released by $CD90^+$ hepatocytes in the form of exosomes. The released H19 induces the upregulation of angiogenesis-related genes, such as *VEGF*, *VEGFR*, and *ICAM* in HUVECs. The results of our current study revealed that HUVECs exposed to ox-LDL had lower levels of H19. ICA promoted H19 expression in HUVECs. Furthermore, we found that low expression of H19 could reverse ICA-induced EndMT inhibition. These findings revealed the involvement of H19-mediated signaling in the regulation of EndMT as an underlying mechanism for the endothelial protective action of ICA.

Usually, lncRNAs are used as competing endogenous RNAs (ceRNAs) to regulate microRNAs (miRNAs) competitively, thereby regulating the expression of miRNA target genes.[34,35] To further explore the molecular mechanism of H19 function, we used bioinformatics-based prediction and functional assays and discovered that H19 could directly interact with miR-148b-3p and function as a ceRNA to regulate the expression of ELF5. miR-148b-3p is a non-coding small RNA highly abundant in cells. It regulates many physiological processes and has potential therapeutic significance for many diseases, including cancer and inflammation. Du et al.[36] previously confirmed that inhibition of miR-148b-3p alleviates oxygen-glucose deprivation/reoxygenation-induced apoptosis and oxidative stress in HT22 hippocampal neurons. The ETS transcriptional regulator was discovered by the Frederick National Cancer Institute in the United States. The ETS transcription factor family plays an important role in various physiological processes, including cell proliferation and differentiation, migration and apoptosis, angiogenesis, and organ formation. Previous research has shown that ELF5 inhibits TGF-β-driven EndMT in prostate cancer by repressing SMAD3 activation.[37] Our current study revealed that ICA suppressed EndMT in HUVECs by inhibiting miR-148b-3p expression and enhancing ELF5 expression. A dual-luciferase reporter experiment confirmed that H19 could directly interact with miR-148b-3p and function as a ceRNA to regulate the expression of ELF5 in HUVECs. We further explored whether miR-148b-3p and ELF5 were involved in EndMT in ox-LDL-stimulated AS. In addition, we also confirmed that ICA inhibited the activation of TGF-β, which is essential for EndMT, through the H19 axis. In accordance with our hypothesis, miR-148b-3p upregulation and ELF5 knockdown antagonized the H19-mediated inhibition of EndMT, which might be a critical molecular mechanism involved in ox-LDL-induced EndMT.

In conclusion, our results verified that H19 plays a protective role by regulating EndMT, while ICA exerts protective effects in ox-LDL-stimulated HUVECs. We also determined the mechanisms downstream of H19, including miR-148b-3p/ELF5, which may serve as a promising therapeutic strategy for AS. However, the role and mechanism of H19 in AS still need to be further explored in animal models.

MATERIALS AND METHODS

Cell culture

HUVECs were cultured in endothelial cell culture medium (Ham's F-12K) (CM0122, Procell Life Science and Technology, Wuhan, China), containing 10% fetal bovine serum, 0.05 mg/mL endothelial cell growth supplement, 0.1 mg/mL heparin, and 1% penicillin/streptomycin at 37°C in a 5% CO_2 atmosphere.

Cell treatment

HUVECs were exposed to 200 μg/mL ox-LDL only (Yiyuan Biotechnology, Guangzhou, China), ox-LDL and 10 μM ICA (Weiqi Biotechnology, Sichuan, China), or ox-LDL and 10 μM ICA and galunisertib (lot no. 63191, MedChemExpress, Shanghai, China) for 24 h.

Cell transfection

lncRNA H19 overexpression (pLVX-H19), sh-H19, and empty vectors (pLVX-negative control [NC], sh-NC) were prepared by LandM Biotechnology (Guangzhou, China). miR-148b-3p mimics, miRNA NC (miR-NC), and si-ELF5 were prepared by GenePharma Technology (Jiangsu, China). HUVECs were seeded in 24-well plates and transfected according to the manufacturer's instructions.

Wound-healing assay

Cells in the logarithmic growth phase were seeded in six-well plates, and the cell density was adjusted to 4×10^5 cells/mL. Cells were cultured in a CO_2 incubator with 5% CO_2 at 37°C for 24 h. After forming a single layer of fusion, scratches were introduced, and they were rinsed with phosphate-buffered saline three times to remove suspended cells. Then, the cells were continuously cultured in serum-free medium for 24 h, imaged using an optical microscope (Olympus, Beijing, China), and the scratch width at the same position was recorded. ImageJ software was used to measure the scratch area at different times.

Transwell assay

Cells were digested and the culture medium was discarded. Then, a serum-free medium containing bovine serum albumin (BSA) was used to resuspend the cells. In detail, 500 μL of the endothelial cell culture medium was added to the lower chamber. Then, 4% paraformaldehyde was added for fixation at 20°C–25°C for 15 min, and 0.1% crystal violet solution was used at the same temperature for 10 min after air-drying. Eventually, the cells within the upper chamber

Figure 7. ELF5 downregulation reversed H19-mitigated EndMT in ox-LDL-treated HUVECs

Cells were transfected with H19 plasmids or si-ELF5 and exposed to ox-LDL. (A–H) After that, the expression levels of H19, ELF5, CD31, VE-cadherin, α-SMA, and S100A4 in HUVECs were determined using western blot analysis or quantitative real-time PCR. (I and J) Cell migration capacity was measured using wound-healing (I) and transwell assays (J). $^*p < 0.05$, $^{**}p < 0.01$ versus pLVX-NC+si-NC group; $^{\#}p < 0.05$, $^{\#\#}p < 0.01$ versus pLVX-H19+si-NC group; n = 3. Measurement data are expressed as mean ± SD. Scale bars, 100 μm.

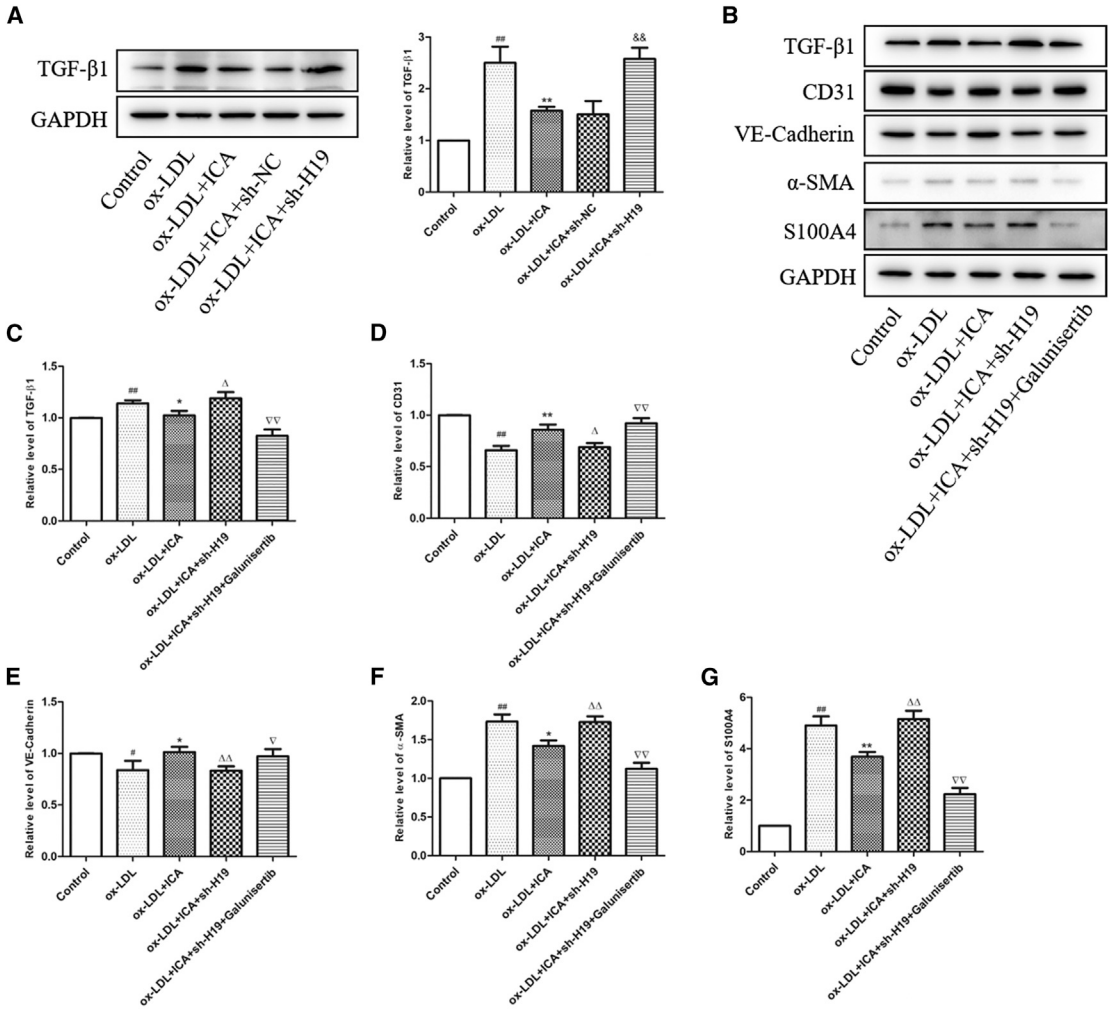

Figure 8. ICA inhibited the expression of TGF-β through H19, and galunisertib reversed the promoting effect of sh-H19 on EndMT

(A) Cells were transfected with sh-H19 and exposed to ox-LDL (with or without ICA); western blot analysis was performed to detect the expression of transforming growth factor-β (TGF-β) in HUVECs. (B–G) After adding galunisertib, the expression of TGF-β, CD31, VE-cadherin, α-SMA, and S100A4 in HUVECs was also determined using western blot analysis. $^{\#}p < 0.05$, $^{\#\#}p < 0.01$ versus control group; $^{*}p < 0.05$, $^{**}p < 0.01$ versus ox-LDL group; $^{\Delta}p < 0.05$, $^{\Delta\Delta}p < 0.01$ versus ox-LDL+ICA group; $^{\nabla}p < 0.05$, $^{\nabla\nabla}p < 0.01$ versus ox-LDL+ICA+sh-H19 group; $^{\&}p < 0.05$, $^{\&\&}p < 0.01$ versus ox-LDL+ICA+sh-NC group; n = 3. Measurement data are expressed as mean ± SD.

were removed with a cotton swab, and the number of cells in the lower chamber was examined in five random image fields.

Luciferase reporter assay

The chemically synthesized H19 and the 3′ UTR of the ELF5 fragment containing the miR-148b-3p binding site and mutated binding site were cloned into the psiCHECK-2 luciferase vector. Transfection was performed using a Lipofectamine 2000 kit (Invitrogen, Carlsbad, CA, USA), according to the manufacturer's instructions, and the recombinant reporter vector and miR-148b-3p mimic or NC mimic were co-transfected into 293T cells (American Type Culture Collection [ATCC], Manassas, VA, USA). After transfection for 48 h, the luciferase activity of the samples was detected using the Dual-Luciferase reporter assay system (Promega, Madison, WI, USA).

Western blot analysis

Lysates of cells were prepared as representatives of total protein extracts. The protein extracts were centrifuged at 12,000 × *g* for 15 min, and the supernatant was collected. Then, the bicinchoninic acid (BCA) protein assay kit (lot no. B68010, Yeasen Biotech, Shanghai, China) was used to detect the protein content. After that, the samples were boiled with 5× sodium dodecyl sulfate-polyacrylamide gel electrophoresis (SDS-PAGE) loading buffer to denature the proteins. Proteins were separated by 10% SDS-PAGE, and the protein amount in each lane was 40 μg. The proteins were then transferred onto polyvinylidene fluoride (PVDF) membranes and incubated with TBST containing 5% BSA for 1 h at 20°C–25°C. The PVDF membranes were probed overnight with CD31 (lot no. 3528S, Cell Signaling Technology, Danvers, MA, USA), VE-cadherin

(lot no. 2500S, Cell Signaling Technology), α-SMA (lot no. 19245S, Cell Signaling Technology), S100A4 (lot no. 13018S, Cell Signaling Technology), and TGF-β (lot no. A18692, ABclonal Biotech, Wuhan, China) primary antibodies at 4°C. After washing three times with TBST, the membranes were incubated with horseradish peroxidase (HRP)-labeled secondary antibody (dilution ratio of 1:5,000, lot no. 33101ES60, Yeasen Biotech) for 1 h at 20°C–25°C. Afterward, enhanced chemiluminescence (ECL) reagent (Absin Biotech, Shanghai, China) was added to the membranes, which were then incubated for 5 min in the dark. Images of the bands were taken using a Tanon imaging system (Bioscience Biotech, Beijing, China). ImageJ software (Bio-Rad, Hercules, CA, USA) was used to analyze the gray value of each protein band and calculate the relative ratio by comparing each band intensity with that of the internal reference (GAPDH).

Quantitative real-time polymerase chain reaction (PCR)

After the cells were treated with different factors, the medium was discarded, and the total RNA was extracted using a general total RNA rapid extraction kit (R1051, Dongsheng Biotech, Guangzhou, China). The content and purity were determined using ultraviolet spectrophotometry (Purkinje General Instrument, Beijing, China). cDNA was synthesized using an All-in-One first-strand cDNA synthesis kit (N20726, TransGen Biotech, Beijing, China) or a miRNA first-strand cDNA synthesis kit (N10824, TransGen Biotech). Quantitative real-time PCR was performed using an all-in-one qPCR mix kit (N10426, TransGen Biotech). GAPDH and U6 were used as endogenous references. The sequences of primers for quantitative real-time PCR are shown in Table S1. The relative expression was calculated using the $2^{-\Delta\Delta Ct}$ method.

Statistical analysis

Experimental data are presented as the mean ± standard deviation (SD). Statistical differences between groups were analyzed using the Student's t test. GraphPad Prism 7.0 software was used for statistical analysis. $p < 0.05$ indicated statistically significant differences.

SUPPLEMENTAL INFORMATION

Supplemental Information can be found online at https://doi.org/10.1016/j.omtn.2020.11.021.

ACKNOWLEDGMENTS

We would like to thank Editage for English language editing. This work was supported by the National Natural Science Foundation of China (grant no. 81773934).

AUTHOR CONTRIBUTIONS

S.L. designed and performed the experiments and wrote the manuscript; L.R. revised the manuscript; and D.X., M.L., Y.Z., Q.L., T.L., and L.R. contributed to experimental work and data analysis. All authors have read and approved the final version of the manuscript.

DECLARATION OF INTERESTS

The authors declare no competing interests.

REFERENCES

1. Laslett, L.J., Alagona, P., Jr., Clark, B.A., 3rd, Drozda, J.P., Jr., Saldivar, F., Wilson, S.R., Poe, C., and Hart, M. (2012). The worldwide environment of cardiovascular disease: prevalence, diagnosis, therapy, and policy issues: a report from the American College of Cardiology. J. Am. Coll. Cardiol. *60* (25, Suppl), S1–S49.
2. Carr, S., Farb, A., Pearce, W.H., Virmani, R., and Yao, J.S. (1996). Atherosclerotic plaque rupture in symptomatic carotid artery stenosis. J. Vasc. Surg. *23*, 755–765.
3. Evrard, S.M., Lecce, L., Michelis, K.C., Nomura-Kitabayashi, A., Pandey, G., Purushothaman, K.R., d'Escamard, V., Li, J.R., Hadri, L., Fujitani, K., et al. (2016). Endothelial to mesenchymal transition is common in atherosclerotic lesions and is associated with plaque instability. Nat. Commun. *7*, 11853.
4. Chen, P.Y., Qin, L., Baeyens, N., Li, G., Afolabi, T., Budatha, M., Tellides, G., Schwartz, M.A., and Simons, M. (2015). Endothelial-to-mesenchymal transition drives atherosclerosis progression. J. Clin. Invest. *125*, 4514–4528.
5. Boström, K.I., Yao, J., Guihard, P.J., Blazquez-Medela, A.M., and Yao, Y. (2016). Endothelial-mesenchymal transition in atherosclerotic lesion calcification. Atherosclerosis *253*, 124–127.
6. Chen, P.Y., Schwartz, M.A., and Simons, M. (2020). Endothelial-to-mesenchymal transition, vascular inflammation, and atherosclerosis. Front. Cardiovasc. Med. *7*, 53.
7. Mo, Z.T., Liao, Y.L., Zheng, J., and Li, W.N. (2020). Icariin protects neurons from endoplasmic reticulum stress-induced apoptosis after OGD/R injury via suppressing IRE1α-XBP1 signaling pathway. Life Sci. *255*, 117847.
8. Hu, L., Liu, F., Li, L., Zhang, L., Yan, C., Li, Q., Qiu, J., Dong, J., Sun, J., and Zhang, H. (2020). Effects of icariin on cell injury and glucocorticoid resistance in BEAS-2B cells exposed to cigarette smoke extract. Exp. Ther. Med. *20*, 283–292.
9. Wei, J.W., Huang, K., Yang, C., and Kang, C.S. (2017). Non-coding RNAs as regulators in epigenetics (Review). Oncol. Rep. *37*, 3–9.
10. Zhou, T., Ding, J.W., Wang, X.A., and Zheng, X.X. (2016). Long noncoding RNAs and atherosclerosis. Atherosclerosis *248*, 51–61.
11. Brannan, C.I., Dees, E.C., Ingram, R.S., and Tilghman, S.M. (1990). The product of the H19 gene may function as an RNA. Mol. Cell. Biol. *10*, 28–36.
12. Li, D.Y., Busch, A., Jin, H., Chernogubova, E., Pelisek, J., Karlsson, J., Sennblad, B., Liu, S., Lao, S., Hofmann, P., et al. (2018). H19 induces abdominal aortic aneurysm development and progression. Circulation *138*, 1551–1568.
13. Zhu, Y., Ni, T., Lin, J., Zhang, C., Zheng, L., and Luo, M. (2019). Long non-coding RNA H19, a negative regulator of microRNA-148b-3p, participates in hypoxia stress in human hepatic sinusoidal endothelial cells via NOX4 and eNOS/NO signaling. Biochimie *163*, 128–136.
14. Zhang, H., Ye, Q., Du, Z., Huang, M., Zhang, M., and Tan, H. (2018). miR-148b-3p inhibits renal carcinoma cell growth and pro-angiogenic phenotype of endothelial cell potentially by modulating FGF2. Biomed. Pharmacother. *107*, 359–367.
15. Lapinskas, E.J., Svobodova, S., Davis, I.D., Cebon, J., Hertzog, P.J., and Pritchard, M.A. (2011). The Ets transcription factor *ELF5* functions as a tumor suppressor in the kidney. Twin Res. Hum. Genet. *14*, 316–322.
16. Lapinskas, E.J., Palmer, J., Ricardo, S., Hertzog, P.J., Hammacher, A., and Pritchard, M.A. (2004). A major site of expression of the ets transcription factor Elf5 is epithelia of exocrine glands. Histochem. Cell Biol. *122*, 521–526.
17. Mahler, G.J., Farrar, E.J., and Butcher, J.T. (2013). Inflammatory cytokines promote mesenchymal transformation in embryonic and adult valve endothelial cells. Arterioscler. Thromb. Vasc. Biol. *33*, 121–130.
18. Xu, X., Friehs, I., Zhong Hu, T., Melnychenko, I., Tampe, B., Alnour, F., Iascone, M., Kalluri, R., Zeisberg, M., Del Nido, P.J., and Zeisberg, E.M. (2015). Endocardial fibroelastosis is caused by aberrant endothelial to mesenchymal transition. Circ. Res. *116*, 857–866.
19. Ranchoux, B., Antigny, F., Rucker-Martin, C., Hautefort, A., Péchoux, C., Bogaard, H.J., Dorfmüller, P., Remy, S., Lecerf, F., Planté, S., et al. (2015). Endothelial-to-mesenchymal transition in pulmonary hypertension. Circulation *131*, 1006–1018.
20. Yao, Y., Jumabay, M., Ly, A., Radparvar, M., Cubberly, M.R., and Boström, K.I. (2013). A role for the endothelium in vascular calcification. Circ. Res. *113*, 495–504.
21. Li, J., Xiong, J., Yang, B., Zhou, Q., Wu, Y., Luo, H., Zhou, H., Liu, N., Li, Y., Song, Z., and Zheng, Q. (2015). Endothelial cell apoptosis induces TGF-β signaling-dependent

host endothelial-mesenchymal transition to promote transplant arteriosclerosis. Am. J. Transplant. *15*, 3095–3111.

22. Cheng, S.L., Shao, J.S., Behrmann, A., Krchma, K., and Towler, D.A. (2013). Dkk1 and MSX2-Wnt7b signaling reciprocally regulate the endothelial-mesenchymal transition in aortic endothelial cells. Arterioscler. Thromb. Vasc. Biol. *33*, 1679–1689.

23. Kim, M., Choi, S.H., Jin, Y.B., Lee, H.J., Ji, Y.H., Kim, J., Lee, Y.S., and Lee, Y.J. (2013). The effect of oxidized low-density lipoprotein (ox-LDL) on radiation-induced endothelial-to-mesenchymal transition. Int. J. Radiat. Biol. *89*, 356–363.

24. Xiao, H.B., Sui, G.G., and Lu, X.Y. (2017). Icariin improves eNOS/NO pathway to prohibit the atherogenesis of apolipoprotein E-null mice. Can. J. Physiol. Pharmacol. *95*, 625–633.

25. Wang, Y., Wang, Y.S., Song, S.L., Liang, H., and Ji, A.G. (2016). Icariin inhibits atherosclerosis progress in Apoe null mice by downregulating CX3CR1 in macrophage. Biochem. Biophys. Res. Commun. *470*, 845–850.

26. Fang, J., and Zhang, Y. (2017). Icariin, an anti-atherosclerotic drug from Chinese medicinal herb horny goat weed. Front. Pharmacol. *8*, 734.

27. Zhang, W.P., Bai, X.J., Zheng, X.P., Xie, X.L., and Yuan, Z.Y. (2013). Icariin attenuates the enhanced prothrombotic state in atherosclerotic rabbits independently of its lipid-lowering effects. Planta Med. *79*, 731–736.

28. Hu, Y., Li, H., Liu, K., Zhang, Y., Ren, L., and Fan, Z. (2018). Protective effects of icariin on human vascular endothelial cells induced by oxidized low-density lipoprotein via modulating caspase-3 and Bcl-2. Mol. Med. Rep. *17*, 6835–6839.

29. Wang, Y.K., and Huang, Z.Q. (2005). Protective effects of icariin on human umbilical vein endothelial cell injury induced by H_2O_2 in vitro. Pharmacol. Res. *52*, 174–182.

30. Xiao-Hong, D., Chang-Qin, X., Jian-Hua, H., Wen-Jiang, Z., and Bing, S. (2013). Icariin delays homocysteine-induced endothelial cellular senescence involving activation of the PI3K/AKT-eNOS signaling pathway. Pharm. Biol. *51*, 433–440.

31. Shima, H., Kida, K., Adachi, S., Yamada, A., Sugae, S., Narui, K., Miyagi, Y., Nishi, M., Ryo, A., Murata, S., et al. (2018). Lnc RNA *H19* is associated with poor prognosis in breast cancer patients and promotes cancer stemness. Breast Cancer Res. Treat. *170*, 507–516.

32. Liu, Y., He, A., Liu, B., Huang, Z., and Mei, H. (2019). Potential role of lncRNA H19 as a cancer biomarker in human cancers detection and diagnosis: a pooled analysis based on 1585 subjects. BioMed Res. Int. *2019*, 9056458.

33. Conigliaro, A., Costa, V., Lo Dico, A., Saieva, L., Buccheri, S., Dieli, F., Manno, M., Raccosta, S., Mancone, C., Tripodi, M., et al. (2015). $CD90^+$ liver cancer cells modulate endothelial cell phenotype through the release of exosomes containing H19 lncRNA. Mol. Cancer *14*, 155.

34. Yoon, J.H., Abdelmohsen, K., Srikantan, S., Yang, X., Martindale, J.L., De, S., Huarte, M., Zhan, M., Becker, K.G., and Gorospe, M. (2012). lincRNA-p21 suppresses target mRNA translation. Mol. Cell *47*, 648–655.

35. Kallen, A.N., Zhou, X.B., Xu, J., Qiao, C., Ma, J., Yan, L., Lu, L., Liu, C., Yi, J.S., Zhang, H., et al. (2013). The imprinted H19 lncRNA antagonizes let-7 microRNAs. Mol. Cell *52*, 101–112.

36. Du, Y., Ma, X., Ma, L., Li, S., Zheng, J., Lv, J., Cui, L., and Lv, J. (2020). Inhibition of microRNA-148b-3p alleviates oxygen-glucose deprivation/reoxygenation-induced apoptosis and oxidative stress in HT22 hippocampal neuron via reinforcing Sestrin2/Nrf2 signalling. Clin. Exp. Pharmacol. Physiol. *47*, 561–570.

37. Yao, B., Zhao, J., Li, Y., Li, H., Hu, Z., Pan, P., Zhang, Y., Du, E., Liu, R., and Xu, Y. (2015). Elf5 inhibits TGF-β-driven epithelial-mesenchymal transition in prostate cancer by repressing SMAD3 activation. Prostate *75*, 872–882.